Article

Not peer-reviewed version

Sedimentary Stylolites Roughness Inversion Enables the Quantification the Eroded Thickness of Deccan Trap Above the Bagh Group, Narmada Basin, India

Dhiren Kumar Ruidas * , Nicolas E. Beaudoin , Srabani Thakur , Aniruddha Musib , Gourab Dey

Posted Date: 4 June 2025

doi: 10.20944/preprints202506.0230.v1

Keywords: Stylolite; Bagh Group; Deccan Trap; FPS; BPS; Paleodepth

 doi:10.20944/preprints202506.0230.v1

Article

Sedimentary Stylolites Roughness Inversion Enables the Quantification the Eroded Thickness of Deccan Trap Above the Bagh Group, Narmada Basin, India

Dhiren Kumar Ruidas [1,*], Nicolas Beaudoin [2], Srabani Thakur [1], Aniruddha Musib [1] and Gourab Dey [3]

[1] Department of Geology, Chunaram Gobinda Memorial Government College, Purulia, India
[2] Laboratoire des Fluides Complexes et Leurs Réservoirs, Universite de Pau et des Pays de l'Adour, E2S UPPA, CNRS, LFCR, 64000 Pau, France
[3] Department of Earth Sciences, IIT Kanpur, India
* Correspondence: dhiren.geol@gmail.com

Abstract: Stylolites, common dissolution surfaces in carbonate rocks, form due to localized stress-induced pressure-solution during burial compaction or tectonic contraction. Their morphology and growth are influenced by dissolution kinetics, rock heterogeneity, clay content, burial depth, stress evolution, diagenesis, and pore fluid availability. This study applies the SRIT, a proven paleopizometer that quantifies the principal vertical stress ($\sigma_v=\sigma_1$) prevailing in strata in the last steps of bedding-parallel stylolites (BPS) formation, to the Late Cretaceous Bagh Group carbonates in the Narmada Basin, India, to estimate their burial paleo-depth. Using Fourier Power Spectrum (FPS) we obtained 18 σ_1 values from a collection of 30 samples enabling to estimate paleo-burial depths for the Bagh Group ranging from 660 to 1320 meters. As the Bagh Group burial history is unknown, but as there is no subsequent sedimentary deposition above it, we relate this ca. 1 km burial depth to the now eroded thickness of the deposits related to Deccan volcanism at the end of the Cretaceous time. This research highlights the robustness of SRIT for reconstructing burial histories in carbonate sequences, particularly emphasizing the suitability of "suture and sharp peak" stylolite types for accurate depth estimations. It also showcases that SRIT can be a reliable way to reconstruct the thickness of eroded deposits in well-constrained geological history.

Keywords: stylolite; Bagh Group; Deccan Trap; FPS; BPS; paleodepth

1. Introduction

Stylolites are rough dissolution surfaces commonly found in carbonate rocks within sedimentary basins formed by localized stress-induced pressure-solution during burial-related compaction or tectonic contraction (Stockdale 1921, Railsback 1993, Toussaint et al., 2018, Koehn et al., 2016). They are visible in cross-section as serrated lines or ridges due to the accumulation of less soluble materials (clay, mica, and oxides) with asperities ranging from micrometers to centimeters (Park and Schot, 1968). Stylolite growth and morphology are rate-dependent, governed by dissolution kinetics (Stockdale, 1943), heterogeneity distribution, and clay content (Renard et al., 2004). Furthermore, burial depth, basin stress evolution, diagenetic overprinting, and the availability of pore fluids also influence stylolite formation (Beaudoin et al, 2019 and Magni et al., 2025). Depending on their permeability and sealing properties, stylolites can either accelerate diagenetic reactions by acting as fluid conduits, have no impact, or inhibit reactions by functioning as barriers, thereby influencing the spatial distribution of diagenetic products (Gomez-Rivas et al., 2022, Heap et al., 2014, 2018).

The roughness is defined as the difference in height (dh) between two points, separated by a defined horizontal distance (dx) along the stylolite track. Stylolite track roughness, characterized by

 doi:10.20944/preprints202506.0230.v1

its scale-invariant (self-affine) geometry in 1D, serves as a valuable paleo-stress indicator because its final form reflects the ambient stress magnitude at fossilization i.e. the time pressure-dissolution stopped, independent of strain rate or lithology, effectively capturing a snapshot of those past conditions (Renard et al., 2004; Schmittbuhl et al., 2004). The Stylolite Roughness Inversion Technique (SRIT), a recent method leveraging stylolite roughness as a paleopiezometer, quantifies principal vertical stress ($\sigma 1$) and has been applied to bedding-parallel stylolites (BPS) to estimate the maximum burial depth. Not only is this the case when there are no tectonics (e.g. Ebner et al., 2009b; Rolland et al., 2012; Beaudoin et al., 2019), but it also provides access to the maximum pre-contraction depth for strata involved in Fold-and-Thrust Belt (Beaudoin et al., 2016, 2020, 2025; Labeur et al., 2021, 2024; Bah et al., 2023, Zeboudj et al., 2023). Over the past decades, efforts were dedicated to validate SRIT in various environments against 1) comparison with indirect measurements of the depth (Beaudoin et al., 2019), 2) comparison to direct age measurements in structures developed after $\sigma 1$ was no longer vertical (Beaudoin et al., 2020, Labeur et al., 2024) and 3) by direct measurement of the temperature at which BPS developed (Beaudoin et al., 2025).

This research aims to estimate burial depth in carbonate rocks using the Stylolite Roughness Inversion Technique (SRIT) on bedding parallel stylolites (BPS) from the Bagh Group of the Narmada Basin, India, which allows for the determination of burial paleo-depth in rocks that were affected by stylolitization when subjected to vertical stress but with an unknown overburden history. The burial depth of the host carbonates is calculated by reconstructing vertical stress from BPS data using the Fourier power spectrum (FPS) analysis (Karcz and Scholz, 2003; Renard et al., 2004; Schmittbuhl et al., 2004; Ebner et al., 2009a, 2009b; Rolland et al., 2014; Beaudoin et al., 2016; Bertotti et al., 2017; Beaudoin et al., 2020), and the implication of these depths is further discussed with respect to the diagenetic and to the geological history of the area.

2. Geological Context

The Narmada Graben, situated along the northern flank of the Satpura horst, stands out for its elevated heat flow (Shanker, 1991). This tectonic configuration, with Satpura forming a horst and the adjacent Narmada and Tapi valleys manifesting as grabens (Figure 1B,C), has been substantiated by seismic refraction and wide-angle reflection studies (Tewari, 2001). The bounding faults of the Narmada Graben are steep, dipping at 70°–80° (Shanker, 1987), and show a cumulative displacement of around 1500–1800 meters (Mishra & Ravi Kumar, 1998).

The carbonate sequence of Bagh Group of the Narmada Basin in central India represents the epicontinental basin deposits of the Late Cretaceous marine inundation of the Indian subcontinent.

 doi:10.20944/preprints202506.0230.v1

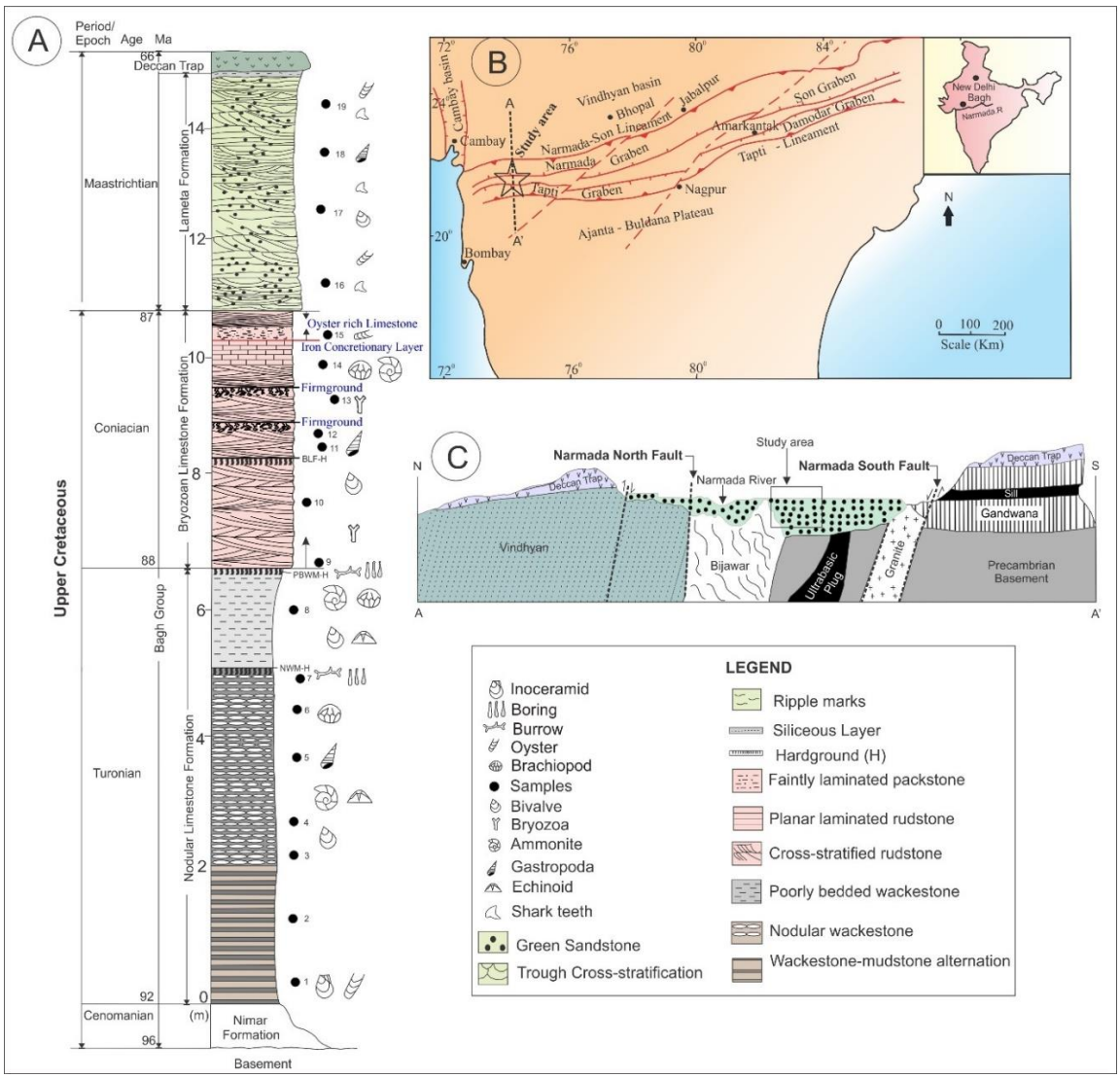

Figure 1. (A) Stratigraphic column for Upper Cretaceous Bagh Group and Lameta Formation with Macro-Micro facies analysis and black circle locate the samples used in this study (Ruidas et al., 2020 & 2023). (B) Tectonic elements around the Narmada basin (Valdiya & Sanwal, 2017) and asterisks used in this study area. (C) Simplified cross section of study area, modified from Murthy & Mishra (1981), Valdiya (1973). Note that the thickness of the Deccan Trap is unknown. .

2.1. Lithostratigraphy of the Bagh Group

The Cenomanian fluvio-marine siliciclastic Nimar Formation is overlain by marine carbonates of the Turonian Nodular Limestone Formation and the Coniacian Bryozoan Limestone Formation. At the regional scale, the carbonate deposits are overlain by the Maastrichtian fluvio-marine, siliciclastic Lameta Formation or by flood basalts of the Deccan Traps (Figure 1A), which are absent in the basin.

2.2. Facies Constituting the Carbonate of Bagh Group

The Nodular Limestone Formation is represented by three non-repetitive facies - i) Facies A- Wackestone-mudstone alternations, ii) Facies B- Nodular wackestone and iii) Facies C- Poorly bedded wackestone. The overlying Bryozoan Limestone Formation (also known as Coralline Limestone, Barwah Bryozoan Limestone and Chirakhan Limestone) consists of three facies - i) Facies D- Cross-stratified rudstone, ii) Facies E- Planar laminated rudstone and iii) Facies F- Faintly laminated packstone in ascending order (Ruidas et al, 2020).

 doi:10.20944/preprints202506.0230.v1

Three distinct hardgrounds are present in ascending stratigraphic order: the first (Hardground 1), a 20 cm-thick, brownish to pinkish-yellow, extensively burrowed, bored (by Gastrochaenolites and Trypanites), and encrusted surface atop the nodular wackestone of the Nodular Limestone Formation; the second (Hardground 2), a 20 cm-thick, rust-brown, Fe-oxide impregnated layer at the top of this formation, separating it from the overlying Bryozoan Limestone and exhibiting bored bioclasts (echinoderm and bryozoan remains), Gastrochaenolites burrow erosion, truncation, and encrustation by Chiplonkarina and oysters; and the third (Hardground 3), within the Bryozoan Limestone, atop a cross-stratified bryozoan limestone unit, marked by Fe-oxide impregnated Thalassinoides burrows and transitioning upward into firmgrounds. Brief description and process interpretation of these facies are given below.

Wackestone-mudstone alternations: This facies consists of dark gray to pinkish-gray colored wackestone-mudstone alternations about 1.7 to 3.1 m thick with parallel to wavy bed geometry, characterized by lack primary depositional sedimentary structures and a paucity of fossils with low degree of bioturbation and desiccation cracks. The wackestone beds often contain, pisoid, intraclast and relics of bioclasts such as gastropods, echinoderms, molluscs and forams with abundant calcispheres. A low-energy, upper intertidal to supratidal depositional environment which undergoing frequent subaerial exposures.

Nodular wackestone: Varying in thickness from 1.6m to 2.9m, this facies consists of nodular wackestone, locally grading to packstone, and is distinguished by desiccation cracks, root structures, a rich assemblage of invertebrate fossils (including bored and fragmented shells), in-situ brecciated rootlets, rhizoconcretions with alveolar-septal texture, invertebrate borings, and Thalassinoides burrows. The nodules, primarily composed of lime mudstone and ranging in shape from broadly spherical (3-7 cm diameter) to ellipsoidal, are embedded within a matrix predominantly consisting of micrite rich in well-preserved bioclasts such as gastropods, echinoderms/echinoid spines, and molluscs, reflecting the abundance of micrite and poor sorting of the bioclasts. The low-energy shallow marine platform– tidal flat depositional condition with long periods of subaerial exposure and pedogenesis.

Poorly bedded wackestone: This facies consists of crudely laminated or massive wackestone characterized by distinct flattened nodularity in which nodules are isolated to jointed and wrapped by thick seams of high proportion of argillaceous material. Thickness of facies varies from 1.3m to 2.4 m. exhibits alveolar texture and intensive calichification. Bioclasts, mainly gastropod, bivalve and rare foraminifera, occur in patches and are frequently impregnated by Fe-oxides. A low energy environment of deposition along with pedogenesis during long periods of subaerial exposure.

Cross-stratified rudstone: Reddish-brown to whitish-brown, thick- to thin-bedded rudstones, characterized by trough and planar cross-stratification with a weakly bipolar, flood-tide dominated paleocurrent pattern, comprise these facies, which contains fragmented bryozoans, echinoids, brachiopods, bivalves, and gastropods, is well-sorted with no micrite, and is occasionally bioturbated by Thalassinoides. High-energy depositional environment characteristic of the lower intertidal environment.

Planar laminated rudstone: The facies consists of greenish-gray, planar laminated rudstone, ranging from 20 cm to 1.3 m thick, characterized by dissolved and strongly bored bioclasts with Fe-oxide coatings and intense micritization; microscopic analysis revealed abundant skeletal grains, including fragments of echinoderms (e.g., echinoid spines), bryozoans, gastropods, ostracods, brachiopods, mollusks, and foraminifera, within a matrix containing moderate amounts of feldspar and quartz, along with 10-25% glauconite. A high-energy depositional condition of lower intertidal depositional setting.

Faintly laminated packstone: The facies, ranging from 1 to 1.5m in thickness, is dominantly composed of poorly bioturbated, fossiliferous packstone with a grain-supported fabric. Well-sorted allochems are a key feature, along with Thalassinoides burrows, abundant meniscus cement, and biomolds. Bioclasts, including bryozoans, echinoderms, and bivalves, make up a significant portion

 doi:10.20944/preprints202506.0230.v1

of the rock (up to 80%). Moderate energy depositional conditions near-shore environments related to lower intertidal deposits.

A low-energy, restricted shallow marine platform-tidal flat system (ranged from supratidal to upper intertidal), subject to periodic subaerial exposures, is inferred for the deposition of the Nodular Limestone. This environment is suggested by the dominance of fine-grained carbonates and mud, the presence of well-preserved small body fossils, and the overlying carbonate units, which signify a reduction or cessation of clastic input in the post-Nimar transgressive depositional system. On the other hand, the presence of abundant cross-stratified/plane-laminated rudstone with siliciclastics, rare mud content, and well-sorted bioclasts in the Bryozoan Limestone provides strong evidence for a high-energy, shallow marine (lower intertidal channels) depositional environment (Akhtar and Khan 1997; Gangopadhyay and Bardhan 2000; Jaitly and Ajane 2013; Ruidas et al., 2018, 2020). The presence of three hardgrounds within the carbonate sequence, primarily marking surfaces of non-deposition, and the associated pattern of slow water-level rise (transgressive trend) followed by a sharp drop suggest an asymmetric depositional cycle.

3. Material and Methods

3.1. Stylolites in the Carbonate of Bagh Group

A series of 30 bedding-parallel stylolites, sampled at consistent intervals throughout the rock unit (Figure 1A), were acquired for subsequent petrographic investigation, morphology and roughness characterization.

The carbonate rock of the Bagh Group exhibits a dispersed distribution of stylolites, ranging from microscopic to macroscopic. Three distinct stylolite connectivity types—isolated, long-parallel, and anastomosing networks (Figures 2 and 3) determine the potential for fluid flow in rocks, a parameter influenced by not only stylolite morphology but also wavelength, amplitude, and orientation (Magni et al., 2025).

Following the classification of Koehn et al., 2016, we recognized stylolites with diverse morphologies, including seismogram pinning (Class 2) type (Figure 4B), suture and sharp peak (Class 3) type (Figures 4A and 5A,C) and simple wave (Class 4) type (Figures 2C and 5D).

 doi:10.20944/preprints202506.0230.v1

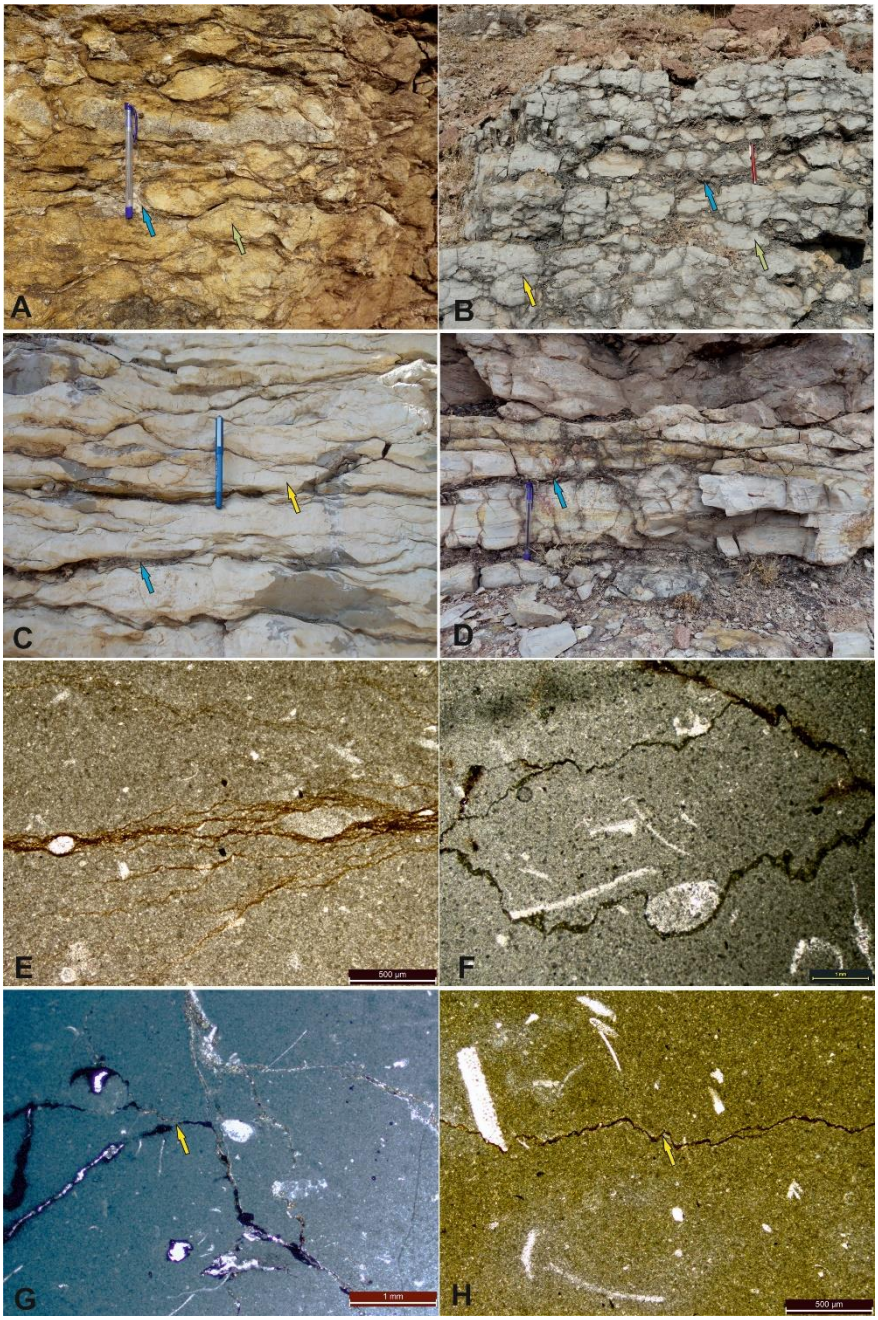

Figure 2. Large-scale parallel stylolites in the Nodular Limestone Formation exhibiting different morphology of stylolites (A, B) anastomosing stylolite networks, (C) Wave-like stylolite, (D) Long layer parallel stylolite (blue arrows mark the mudstone and yellow arrows mark the wakestone); Photomicrograph showing (E, F) anastomosing wave like stylolite in Wackestone and (G, H) anastomosing wave like stylolite in mudstone. The yellow arrow points at a long parallel stylolite. Scale: Pen length 13cm.

 doi:10.20944/preprints202506.0230.v1

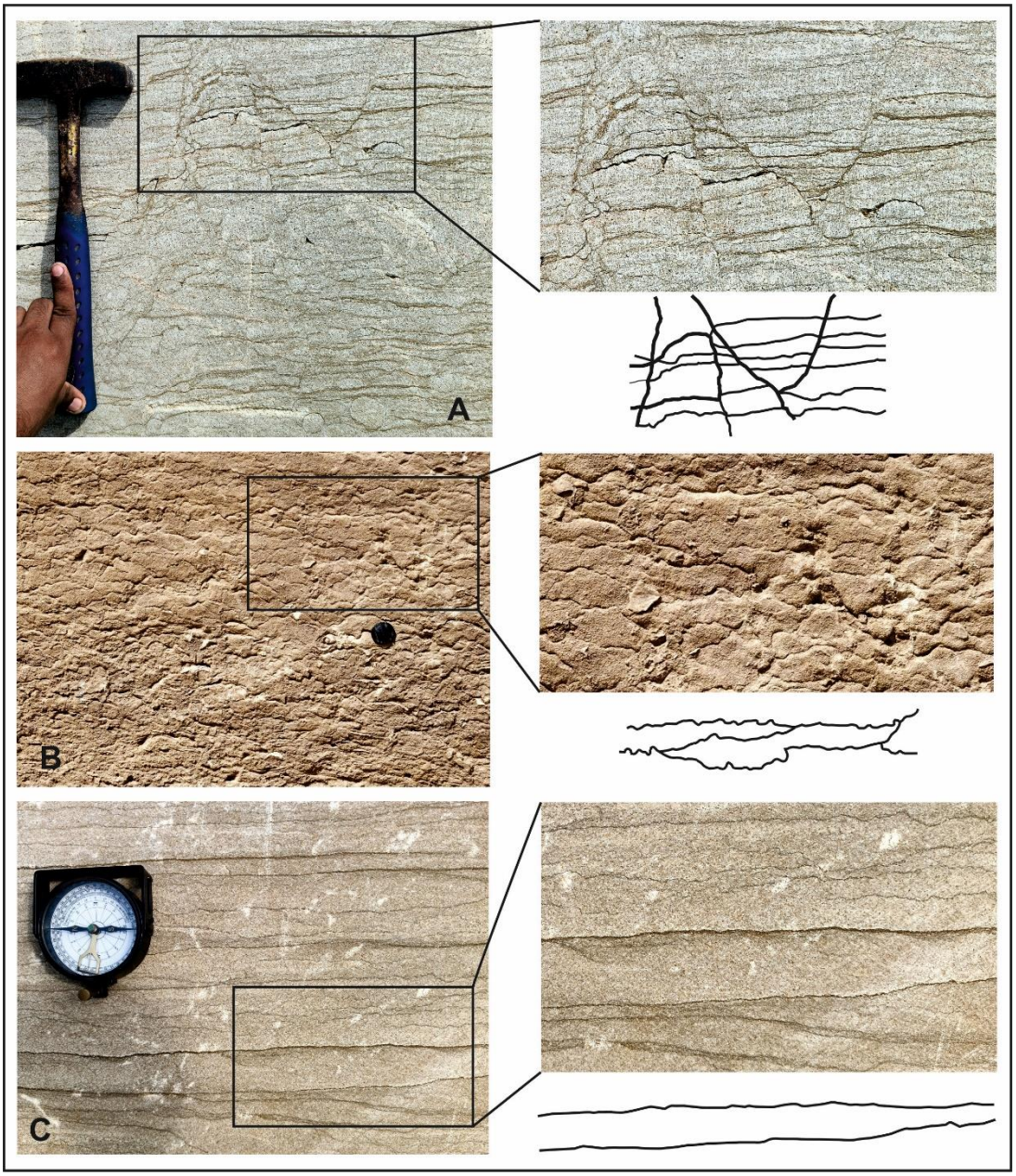

Figure 3. Interconnected stylolite network from an Upper Cretaceous Bagh Group Limestone quarry near Kasdana. Stylolites based on morphology as proposed by Koehn et al., (2016), with close-up cross section view on right-hand side**,** stylolite track drawn for (A) stylolite networks with fracture, (B) anastomosing stylolite networks, and (C) Long layer parallel type stylolite and sketch showing general morphology class characteristics (right-hand side) investigated from the Bryozoan Limestone Formation, Scale: Hammer length 12inches, Lence cover length 4cm diameter, Clinometer length 7cm.

 doi:10.20944/preprints202506.0230.v1

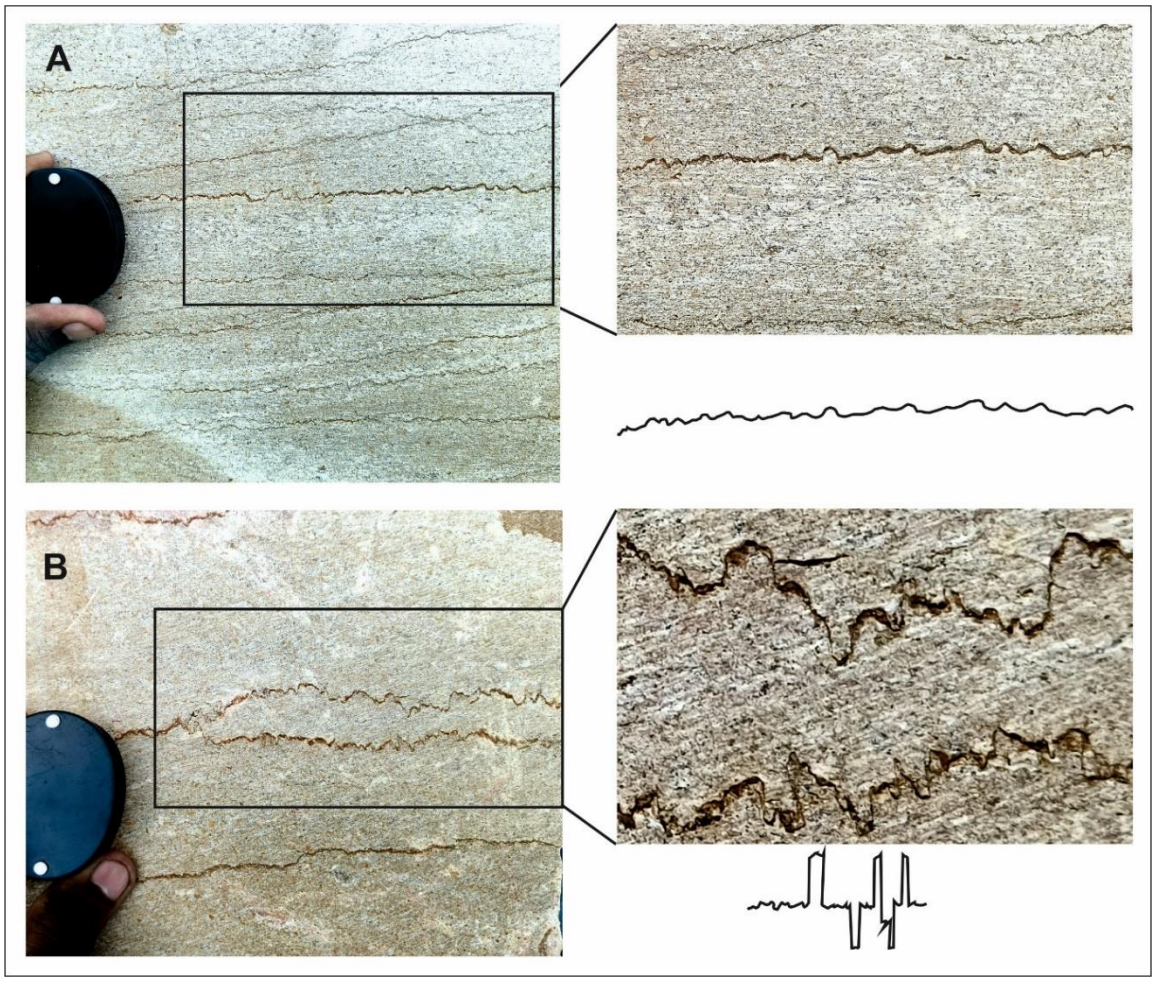

Figure 4. Stylolites based on morphology as proposed by Koehn et al., (2016), with close-up cross section view on right-hand side, stylolite track drawn showing (A) Suture and sharp peak type and (B) seismogram pinning type stylolite and sketch showing general morphology class characteristics (right-hand side) investigated from the Bryozoan Limestone Formation, Scale: Lence cover length 4cm diameter.

 doi:10.20944/preprints202506.0230.v1

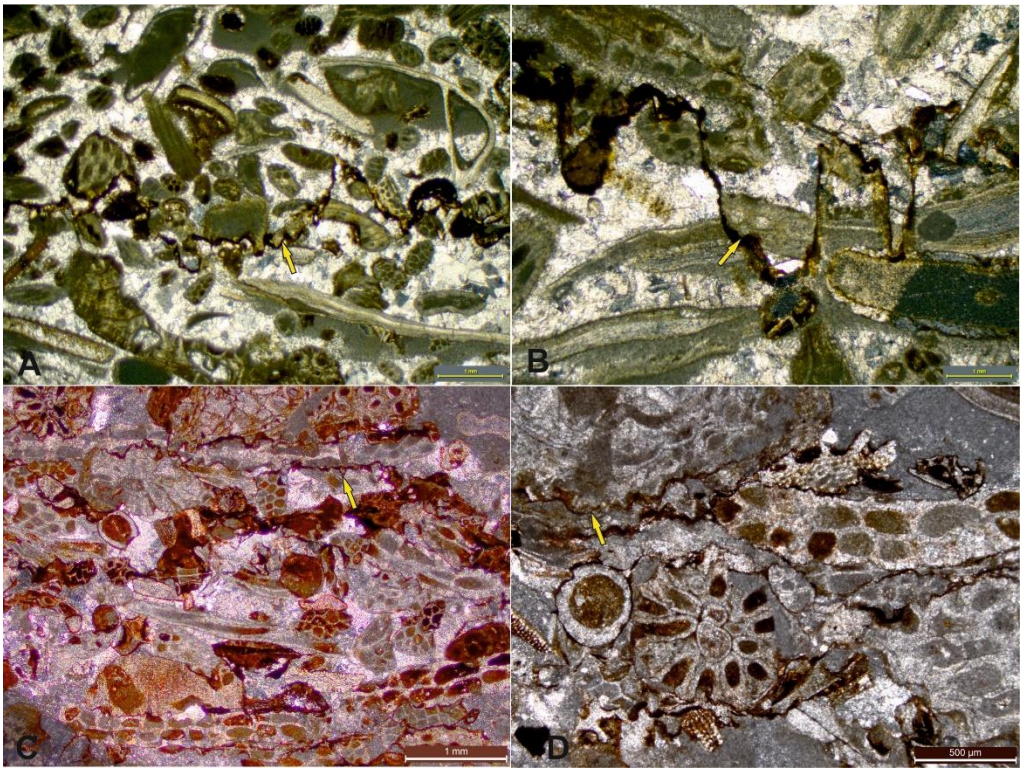

Figure 5. Photomicrograph showing types of stylolite (A) suture and sharp peak type in Packstone, (B) Rectangular layer type stylolite in Rudstone, (C) Suture and sharp peak type in Rudstone, and (D) wave like type in Packstone. The yellow arrow points at a long parallel stylolite.

3.2. Methodology for Stress Inversion

Stylolites mainly develop perpendicular to the maximum principal stress direction (Koehn et al., 2012) that's why on the field stylolite's teeth mainly used to determine the maximum compressive stress axis (Ebner et al., 2009b). Stylolite roughness can be studied as a 2-D track on a polished cross section cut perpendicular to the stylolite's plane (Renard et al., 2004). The roughness, i.e. the difference in height between two consecutive points constitutive of the track can be studied as a signal, with various spatial frequencies corresponding the horizontal distance between the consecutive points (Schmittbuhl et al., 2004). The mathematical relationship between the roughness analysis and the magnitude of the applied normal stress as proposed by Schmittbuhl et al., 2004 and Renard et al., 2004 led to an inversion method popularized under the name SRIT (Stylolite Roughness Inversion Technique, Beaudoin and Lacombe, 2018).

The stylolite's growth balanced between the two stabilizing forces – one is long range elastic fluctuation, and another one is local surface tension – these stabilizing forces are the causes of reduction of Helmholtz free energy, that's why we get flattening surface of the stylolites. A destabilizing force also acts with these due to heterogeneity of the pinning particles in the stylolite surface which increases the Helmholtz free energy and responsible for the formation of teeth and peak of stylolites. (Ebner et al., 2009b; Beaudoin et al., 2019; Schmittbuhl et al., 2004). These impurities of the stylolite surfaces initiate the elastic moduli fluctuation. On large- and small-scale destabilizing forces which create roughness of the materials balance by the surface tension (Ebner et al., 2009b). As the main destabilizing force depends on the scale of observation, there is, in the spectral domain, a characteristic length at which the regime developing roughness switch from being controlled by the elastic forces to being controlled by the Helmhotlz free energy. This length is a key factor named the Crossover length (L_c) which depends on both mean and differential stress under which the roughness developed. In other word, SRIT can return stress magnitude at the time a stylolite stopped developing. In a Fourier domain on a log-log plot, both the roughness controlled by elastic and surface energy are defined by a straight line with a different slope (Schmittbuhl et al., 2004; Beaudoin

 doi:10.20944/preprints202506.0230.v1

et al., 2019; Renard et al., 2004). This slope is defined by the Hurst Coefficient (H), a transferable coefficient depending on the origin of the phenomenon it describes, with capillary effects mainly dominant when H > 1(here mainly 1.1) at short length scale whereas H<1 (Here mainly 0.5) the stress distribution may control the geomorphometry of stylolites during formation at large scale length (Renard et al., 2004).

Here, we studied nearly 30 BPS (Bedding Parallel Stylolites) collected from Kasdana and Karondiya area of Bagh Group, Dhar District, Madhya Pradesh (Figure 1A). The macroscopic stylolites are collected from the perpendicular section of stylolites planes of Bryozoan Limestone. The vertical stress and horizontal stresses i.e. main principal stresses both act perpendicular to the stylolites plane (Ebner et al., 2009b). After collecting the stylolites sample, we washed it and polished it with polishing powder to remove the clay from the samples and then scanned it (3200 dpi). The scanned images are traced through GIMP 2.10.38 application (Figure 6).

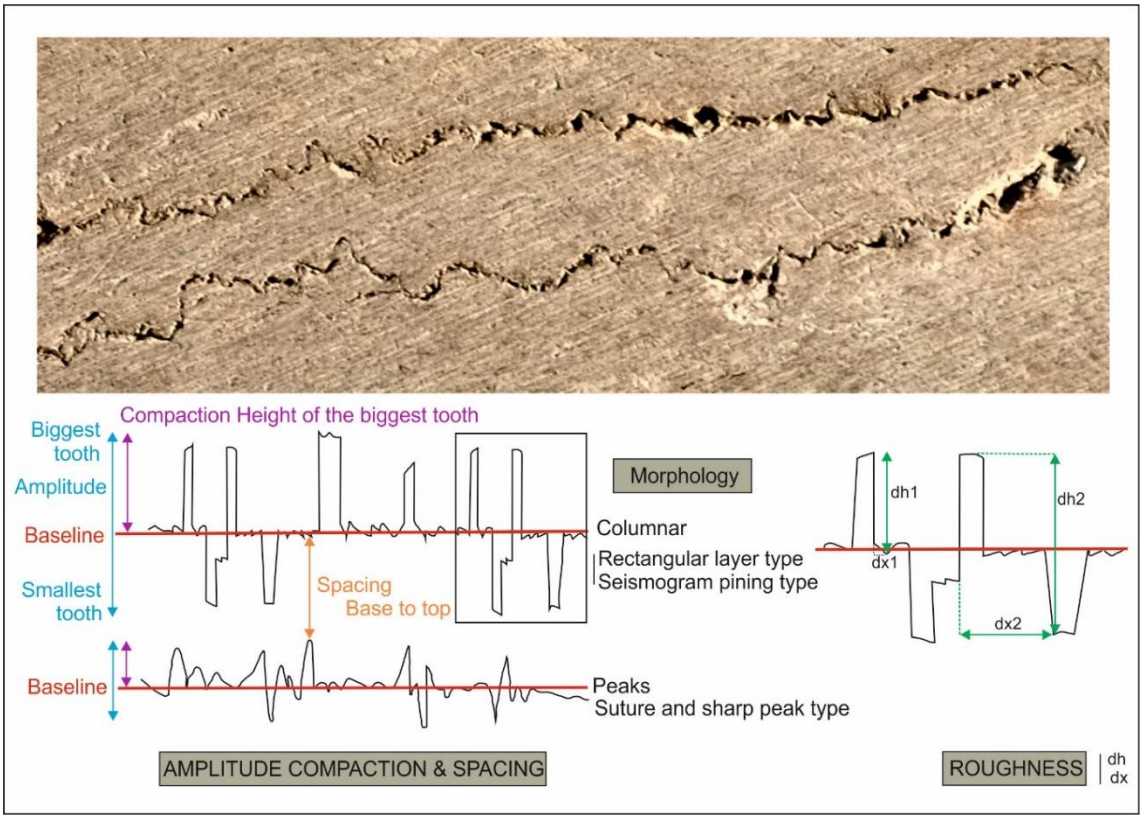

Figure 6. Photograph of stylolites encountered in the Bagh Group, illustrating a sketch that defines the physical and morphological characteristics of stylolites, including amplitude, morphology, roughness and spacing (from Labeur et al., 2024).

In this study, we apply SRIT using Fourier Power Spectrum. As such, the H is determined for the FPS (Fourier Power Spectrum) as a power law exponent of $P(k) = k^{-(1+2H)}$ for 1-D self-affine roughness properties of the materials (Renard et al., 2004). The number of parallel stylolites series get from perpendicular stylolites plane. For each series, the Fourier transformation modulus square (P(k)) is calculated. For 1-D profile removing the noise to get the binned signals by using inverse of the Nyquist-frequency ranges between 1/L spatial frequency and N/2L Nyquist-frequency.

According to Schmittbuhl et al., 2004 and Renard et al., 2004, based on stylolite growth model a generalized Langevin equation was derived with the help of 1st principle of mechanics and thermodynamics and from this it is also described that stylolites growth model interactions between stabilizing forces (surface tension and elastic forces) and disorder of the materials (Ebner et al., 2009). Schmittbuhl et al., 2004 derived an equation based on stress, surface tension and crossover length-

 doi:10.20944/preprints202506.0230.v1

$$L_c = \frac{\gamma E}{\beta \sigma_m \sigma_d} \quad (1)$$

where, L_c is crossover length, E is Young's Modulus, γ is solid-fluid interfacial energy, $\beta = \frac{\upsilon(1-2\upsilon)}{\pi}$ is dimensionless constant. υ is the Poisson's ratio, σ_d and σ_m are differential stress and mean stress respectively.

According to Ebner et al., 2009b, the main principal stress is vertical (σ_{zz}) and rest of the axes are horizontal and lesser value than vertical stress. Where $\sigma_m = \frac{1}{3(\sigma_{zz}+2\sigma_{xx})}$ and $\sigma_d = \sigma_{zz} - \sigma_{xx}$. Assumed that the uniaxial strain was applied so horizontal and vertical component of stress can be related as $\sigma_{xx} = \sigma_{yy} = \left[\frac{\upsilon}{(1-\upsilon)}\right]\sigma_{zz}$. It is also noted that there is an expression of mean and differential stresses as a function of vertical stress component such that $\sigma_m \sigma_d = \alpha \sigma_{zz}^2$ where α is $\frac{1\,(1+\upsilon)(1-2\upsilon)}{3\,(1-\upsilon)(1-\upsilon)}$. So, equation 1 has modified as a function of main vertical stress component, surface tension and surface tension

$$L_c = \frac{\gamma E}{\beta} \times \frac{1}{\alpha \sigma_{zz}^2} \quad (2)$$

In this study, we estimated the Young's modulus (E), which is considered the most uncertain elastic parameter for carbonate rocks (Regnet et al., 2019). To achieve this, we employed a non-destructive technique using the Schmidt hammer, which measures the rebound value (R) of a spring-loaded piston when applied orthogonally to the rock surface. Specifically, we applied the equation proposed by Katz et al., 2000:

$$E = 0.00013 \times R^{3.090704}$$

Lastly, we calculate the paleostress burial depth (z) with the help of lithostatic stress (Main vertical stress) $\sigma_{zz} = \rho g z$ where ρ is density of carbonate rock = 2700 Kg/m^3, g = 9.81 m/s^2 and z is the paleostress depth.

The selection of suture and sharp peak-type stylolites for burial depth estimation is predicated upon the presence of sharp teeth characterized by large-scale roughness, a feature readily digitized and analyzed, thus enhancing the accuracy of depth determination. For maximum paleo-depth determination, suture and sharp peak stylolite types are optimal, whereas seismogram pinning stylolites yield intermediate depth estimations (Beaudoin et al., 2019, Bah et al., 2023). While simple wave-like stylolites, distinguished by their limited roughness and the presence of original layer material, provide effective barriers to fluid flow, their inherent characteristics render them impractical for accurate compaction estimates (Koehn et al., 2016). For optimal SRIT results, it is recommended to avoid the use of simple wave-like stylolites and mudstone host rock textures, which exhibit the greatest variability (Beaudoin et al., 2019).

4. Results

We analyzed mainly 18 samples of BPS (Bedding Parallel Stylolites) by SRIT (Table 1) During our calculation we fixed the Hurst Coefficient values for steep and gentle slope of FPS curve. For steep slopes the lower scale value of H is considered as 1.1 and 0.5 for higher scale gentle slope (Ebner et al., 2009b). Here we mainly rely on the crossover wavelength L_c values by binned data through FPS (Fourier Power Spectrum) curve. L_c values vary from 0.31-1.26 (Figure 7), with no clear relationship to the relative depth of sampling if considering the Bagh Group. For conducting the inversion from L_c to stress, we assumed the horizontal in-plane stress were negligible, we consider γ = 0.23 J/m^2 (Wright et al., 2001) and Poisson's ratio υ = 0.25±0.05 (Clark, 1966). The values for Young Modulus, by far the biggest source of uncertainty in SRIT (Rolland et al., 2014; Beaudoin et al., 2016), were estimated through the rebound value obtained with the Schmidt Hammer. A total of 45 R values were obtained from flat, homogeneous surfaces across 31 samples of Bagh Carbonate rock. These R values are strikingly consistent and ranged from 21 to 22, resulting in calculated Young's moduli between 22 and 25 GPa (Katz et al., 2000).

 doi:10.20944/preprints202506.0230.v1

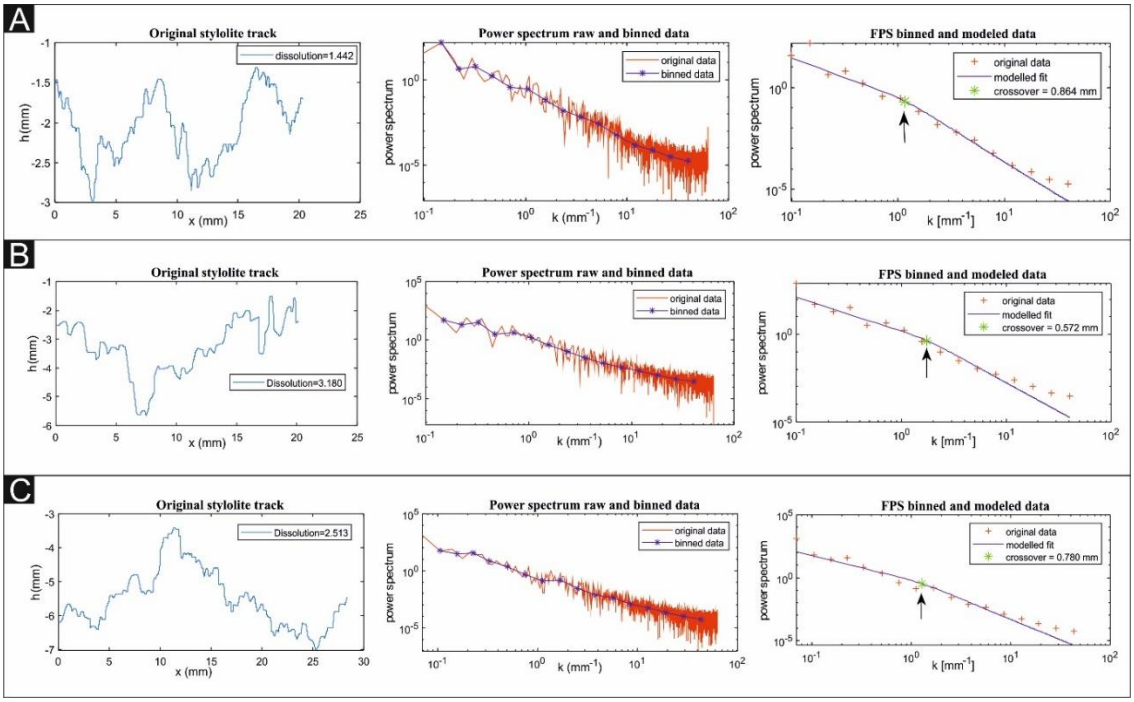

Figure 7. Selected examples demonstrating stylolite roughness inversion techniques. For each case (top left to bottom right): first, stylolite track with estimated minimum dissolution; Next is Fourier Power Spectrum (FPS) analysis including original and binned data following Ebner (2009). Finally, FPS binned data with modelled regression line (blue) under the same Hurst constraints, also yielding Lc (green star). Black arrows mark the crossover length.

Solving equation 4 for each Lc value, we obtain a paleo burial depth varying between 670 -1320 m (rounded to the closest 10 m, excluding the 12% uncertainty, Table 1).

Table 1. Results from the application of the stylolite roughness inversion technique (SRIT) on samples of Bagh Group, Narmada Basin, India.

Sample No.	Stylolite length (mm)	Crossover length (mm)	Paleostress (MPa)	Depth (m)
BG001	20	0.58	26	980
BG002	18	0.41	30	1170
BG003	18	0.32	35	1320
BG004	15	0.34	33	1270
BG005	25	0.75	22	860
BG006	16	0.60	25	960
BG007	20	1.23	17	670
BG008	20	1.23	17	670
BG009	25	0.61	25	950
BG010	25	0.89	20	790
BG011	14	0.55	26	1000
BG012	14	0.34	34	1290
BG013	16	0.39	31	1190
BG014	18	0.47	28	1080
BG015	18	1.27	17	660
BG016	20	0.47	28	1080
BG017	18	0.69	23	900
BG018	30	0.83	21	820

*FFT (First Fourier Transform) Inversion Results using γ = 0.23 J/m2 (Wright et al., 2001), Poisson's ratio υ = 0.25±0.05 (Clark, 1966), E (Young's Modulus) = 25 GPa, ϱ (density) of carbonate rock = 2700 Kg/m3, g = 9.81 m/s2;

 doi:10.20944/preprints202506.0230.v1

Here we put the H (Hurst Coefficient) value as constant i.e. for steep slope 1.1 and gentle slope it is 0.5. All stress and depth values are given without the 12% uncertainty, while Lc values are reported without the 23% uncertainty.

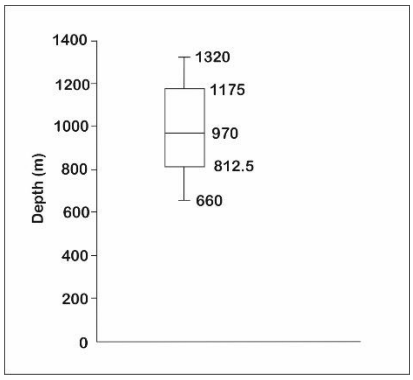

Figure 8. A Box-and-Whisker plot visualizes the burial depth of 18 carbonate rock samples from the Bagh Group. These depths were calculated using stylolite roughness inversion, specifically focusing on bedding-parallel stylolites. The plot displays the minimum, first quartile, median, third quartile, and maximum burial depths at the time pressure solution was active.

5. Interpretation

The morphological variability of stylolites within sedimentary rocks, characterized by wavelength, frequency, and amplitude across multiple scales, exerts a significant influence on both the efficiency of fluid flow along dissolution planes and the accurate estimation of chemical compaction (Andrews and Railsback, 1997, Koehn et al., 2016). The morphology of stylolites is controlled by both growth regimes (Koehn et al., 2016) and the distribution of heterogeneity within the host rock (Andrews & Railsback, 1997). To ensure that the recorded depth throught SRIT is consistent, we analysed suture and sharp peak (Class 3) stylolites (Koehn et al., 2016). In the Late Cretaceous, carbonates of Bagh Group were initially deposited in the basin, due to marine transgression. Subsequently, its properties were altered by bioturbation. As burial progressed (few hundred meters), overburden pressure increased ($\sigma_1 = \sigma_v$), and pressure solution was initiated, leading to the formation of stylolites. As our dataset suggests, stylolitization was intense up to 1000m depth, resulting in extensive stylolitization in the lower layers, marked by closely spaced, well-developed stylolites, reflecting significant volume reduction (Figure 9).

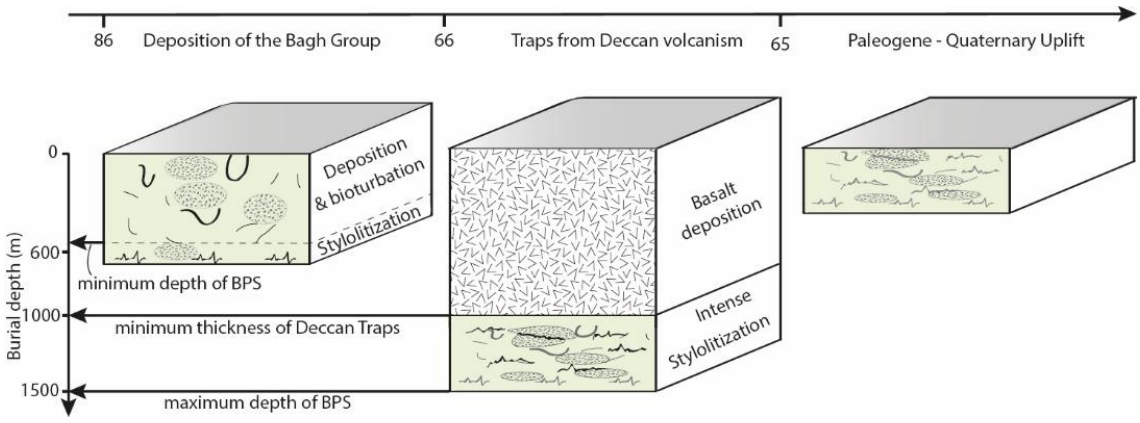

Figure 9. Schematic representation of the bedding-parallel stylolite (BPS) growth at different steps of the host rock burial history. The Bagh Group is represented in light green, with burrows and bioturbation and stylolites. The black colour of these objects represents active development, while grey represents that they are not developing anymore. Depths reported are derived from SRIT applied to BPS.

 doi:10.20944/preprints202506.0230.v1

7. Discussion

Bedding parallel stylolites develop under a vertical principal stress, and stop developing for various reason, including a rise in local fluid pressure (e.g. Bah et al., 2023), decrease of the solubility gradient by clay accumulation (Toussaint et al., 2018), deepening of the strata and accommodation of shortening by more efficient dislocation/recrystallisation mechanisms (Gomez-Rivas et al., 2021), or change in the tectonic stress regime (Lacombe et al., 2021). This case study reconstructed depth ranging from 600 to 1500 m within the 13% uncertainty for the stress calculations (Rolland et al., 2014), and because we do not have independent estimate of the expected maximum burial depth, it is hard to explain why BPS halted their development. Indeed, the Bagh Group is the last formation before the Deccan Traps were deposited (Courtillot et al., 1986). As a large portion of the related lava were eroded since deposition, we know that the studied area was covered (Self et al., 2022), but we do not know what the thickness of this magmatic cover was. Yet, the Bagh Group carbonates' own thickness does not allow to explain the minimal burial depth of 1500 m when BPS stopped to develop. On top of it, one can note that the maximum reconstructed depth is not found only at the bottom of the Bagh Group (BG2-4; BG 12-13, Table 1, Figure 1). So, this range of values probably reflect a sequential stop of BPS activity (e.g. Beaudoin et al., 2025) rather than a synchronous stop at the scale of the whole formation (sensu Ebner et al., 2009b). We propose that the range of depth reconstructed from SRIT, especially at the top of the studied sedimentary column (i.e. 1 km), correspond to a minimum thickness of the Deccan Traps in the study area before it got removed by weathering and erosion consistently with geochemical models at larger scale. Such quantitative estimate, which is a minimum because of potential erosion of the top of the Bagh Group fm. on the one hand and because BPS could have stopped developing before strata reached the maximum burial depth on the other hand, is consistent with independent estimates of the remaining thickness of the traps by the means of geophysics (700m to 2km, Patro and Sarma, 2007). It also provides new constraint on the timescale of stylolite development in nature, showing that the pressure solution can be done rather fast, as the whole population developed during the catastrophic accumulation of the traps, i.e. likely under 600 Kyr (Chenet et al., 2007).

8. Conclusion

The Late Cretaceous carbonate lithologies of the Bagh Group, situated within the Narmada Basin, exhibit a prevalence of bedding-parallel stylolites of variable dimensions. Morphological analysis of the stylolites present in the Bagh Group's carbonate rocks reveals two most distinct categories: (a) suture and sharp peak type stylolites, and (b) simple wave type stylolites.

The application of roughness inversion methodology to these stylolites enables the estimation of sedimentary stylolite formation depth, thereby facilitating the reconstruction of stratigraphic burial history. The principal vertical stress and corresponding burial depth are determined by utilizing the suture and sharp peak-type stylolites, which are dominant in the carbonate rocks in Bagh Group.

The application of the FPS methodology to 18 bedding-parallel stylolite datasets derived from the carbonate lithologies resulted in a heterogeneous distribution of inferred burial depths range from 670 -1320 m, with a median value of 970 meters, independently of the stratigraphic position of samples in the Bagh Group. The calculated depths imply to reevaluate the burial history of the Narmada Basin, with considering an important role of the now eroded Deccan Traps in the area.

Beyond regional implication, this study is the first to rely onto BPS SRIT only to reconstruct burial in a basin, and it clearly illustrates that BPS inversion for vertical stress can be used serve as a gauge for the minimal thickness of eroded formation and can even guide reconstruction of past eruptive events in both intensity and geographical extent.

Author Contributions: The manuscript is a joined effort of D.K.R. and N.B. D.K.R., S.T., G.D. and A.M.: Conceived the study, performed the field work, provided photographs, gathered the data and prepared the first

 doi:10.20944/preprints202506.0230.v1

version of the manuscript. N.B.: Additionally prepared model, modified figures, and prepared the graphs. All authors have read and agreed to the published version of the manuscript.

Acknowledgments: Authors are thankful the CGMGC Purulia and universities for infrastructure facilities. The authors thank Rajesh Dey (Officer in Charge), Abhijit Sarkar and Department Colleagues of CGMGC for infrastructure facilities. AA is thankful to SERB (file no.: EEQ/2023/000086) for financial support. Finally, appreciation goes to Sanjoy Sengupta, Dr. B. C. Roy Engineering College, Durgapur, for facilities the Schmidt hammer test on rock samples.

References

1. Akhtar, K. and Khan, D.A., 1997. A tidal island model for carbonate sedimentation: Karondia Limestone of Cretaceous Narmada basin, India. *Journal Geological Society of India*, *50*(4), pp.481-489.
2. Andrews, L.M. and Railsback, L.B., 1997. Controls on stylolite development: morphologic, lithologic, and temporal evidence from bedding-parallel and transverse stylolites from the US Appalachians. *The Journal of Geology*, *105*(1), pp.59-73.
3. Bah, B., Beaudoin, N.E., Lacombe, O., Girard, J.P., Gout, C., Godeau, N. and Deschamps, P., 2023. Multi-proxy reconstruction of the burial history and porosity evolution of the TOCA carbonate formation in the Lower Congo basin (South West Africa). *Marine and Petroleum Geology*, *148*, p.106018.
4. Beaudoin, N. and Lacombe, O., 2018. Recent and future trends in paleopiezometry in the diagenetic domain: Insights into the tectonic paleostress and burial depth history of fold-and-thrust belts and sedimentary basins. *Journal of Structural Geology*, *114*, pp.357-365.
5. Beaudoin, N., Gasparrini, M., David, M.E., Lacombe, O. and Koehn, D., 2019. Bedding-parallel stylolites as a tool to unravel maximum burial depth in sedimentary basins: Application to Middle Jurassic carbonate reservoirs in the Paris basin, France. GSA Bulletin, 131(7-8), pp.1239-1254.
6. Beaudoin, N., Koehn, D., Lacombe, O., Lecouty, A., Billi, A., Aharonov, E. and Parlangeau, C., 2016. Fingerprinting stress: Stylolite and calcite twinning paleopiezometry revealing the complexity of progressive stress patterns during folding—The case of the Monte Nero anticline in the Apennines, Italy. *Tectonics*, *35*(7), pp.1687-1712.
7. Beaudoin, N., Lacombe, O., Koehn, D., David, M.E., Farrell, N. and Healy, D., 2020. Vertical stress history and paleoburial in foreland basins unravelled by stylolite roughness paleopiezometry: Insights from bedding-parallel stylolites in the Bighorn Basin, Wyoming, USA. Journal of Structural Geology, 136, p.104061.
8. Beaudoin, N.E., Koehn, D., Aharonov, E., Billi, A., Daeron, M. and Boyce, A., 2025. Reconstruction of the Temperature Conditions of Burial-Related Pressure Solution by Clumped Isotopes Validates the Analysis of Sedimentary Stylolites Roughness as a Reliable Depth Gauge. *Minerals*, *15*(1), p.73.
9. Bertotti, G., de Graaf, S., Bisdom, K., Oskam, B., Vonhof, H.B., Bezerra, F.H., Reijmer, J.J. and Cazarin, C.L., 2017. Fracturing and fluid-flow during post-rift subsidence in carbonates of the Jandaíra Formation, Potiguar Basin, NE Brazil. *Basin Research*, *29*(6), pp.836-853.
10. Bhattacharya, B., Halder, K., Jha, S., Mondal, P. and Ray, R., 2021. Stratigraphy, sedimentology and paleontology of late Cretaceous Bagh beds, Narmada Valley, Central India: a review. *Mesozoic Stratigraphy of India: a multi-proxy approach*, pp.623-657.
11. Chenet, A.L., Fluteau, F., Courtillot, V., Gérard, M. and Subbarao, K.V., 2008. Determination of rapid Deccan eruptions across the Cretaceous-Tertiary boundary using paleomagnetic secular variation: Results from a 1200-m-thick section in the Mahabaleshwar escarpment. *Journal of Geophysical Research: Solid Earth*, *113*(B4).
12. Clark, S.P., 1966. *Handbook of physical constants*. Geological society of America.

 doi:10.20944/preprints202506.0230.v1

13. Courtillot, V., Besse, J., Vandamme, D., Montigny, R., Jaeger, J.J. and Cappetta, H., 1986. Deccan flood basalts at the Cretaceous/Tertiary boundary?. *Earth and Planetary Science Letters*, *80*(3-4), pp.361-374.
14. Ebner, M., Koehn, D., Toussaint, R. and Renard, F., 2009a. The influence of rock heterogeneity on the scaling properties of simulated and natural stylolites. *Journal of Structural geology*, *31*(1), pp.72-82.
15. Ebner, M., Koehn, D., Toussaint, R., Renard, F. and Schmittbuhl, J., 2009b. Stress sensitivity of stylolite morphology. *Earth and Planetary Science Letters*, *277*(3-4), pp.394-398.
16. Ehrenberg, S.N., Morad, S., Yaxin, L. and Chen, R., 2016. Stylolites and porosity in a Lower Cretaceous limestone reservoir, onshore Abu Dhabi, UAE. *Journal of Sedimentary Research*, *86*(10), pp.1228-1247.
17. Gangopadhyay, T.K. and Bardhan, S., 2000. Dimorphism and a new record of Barroisiceras De Grossouvre (Ammonoidea) from the Coniacian of Bagh, central India. *Canadian Journal of Earth Sciences*, *37*(10), pp.1377-1387.
18. Gomez-Rivas, E., Butler, R.W., Healy, D. and Alsop, I., 2020. From hot to cold-the temperature dependence on rock deformation processes: an introduction. *Journal of Structural Geology*, *132*, p.103977.
19. Gomez-Rivas, E., Martín-Martín, J.D., Bons, P.D., Koehn, D., Griera, A., Travé, A., Llorens, M.G., Humphrey, E. and Neilson, J., 2022. Stylolites and stylolite networks as primary controls on the geometry and distribution of carbonate diagenetic alterations. *Marine and Petroleum Geology*, *136*, p.105444.
20. Heap, M., Reuschlé, T., Baud, P., Renard, F. and Iezzi, G., 2018. The permeability of stylolite-bearing limestone. *Journal of structural geology*, *116*, pp.81-93.
21. Heap, M.J., Baud, P., Reuschlé, T. and Meredith, P.G., 2014. Stylolites in limestones: Barriers to fluid flow? *Geology*, *42*(1), pp.51-54.
22. Jaitly, A.K. and Ajane, R., 2013. Comments on Placenticeras mintoi (Vredenburg, 1906) from the Bagh Beds (Late Cretaceous), Central India with special reference to turonian nodular limestone horizon. *Journal of the Geological Society of India*, *81*, pp.565-574.
23. Karcz, Z. and Scholz, C.H., 2003. The fractal geometry of some stylolites from the Calcare Massiccio Formation, Italy. *Journal of Structural Geology*, *25*(8), pp.1301-1316.
24. Katz, O., Reches, Z.E. and Roegiers, J.C., 2000. Evaluation of mechanical rock properties using a Schmidt Hammer. *International Journal of rock mechanics and mining sciences*, *37*(4), pp.723-728.
25. Koehn, D., Ebner, M., Renard, F., Toussaint, R. and Passchier, C.W., 2012. Modelling of stylolite geometries and stress scaling. *Earth and Planetary Science Letters*, *341*, pp.104-113.
26. Koehn, D., Renard, F., Toussaint, R. and Passchier, C.W., 2007. Growth of stylolite teeth patterns depending on normal stress and finite compaction. *Earth and Planetary Science Letters*, *257*(3-4), pp.582-595.
27. Koehn, D., Rood, M.P., Beaudoin, N., Chung, P., Bons, P.D. and Gomez-Rivas, E., 2016. A new stylolite classification scheme to estimate compaction and local permeability variations. *Sedimentary Geology*, *346*, pp.60-71.
28. Labeur, A., Beaudoin, N.E., Lacombe, O., Emmanuel, L., Petracchini, L., Daëron, M., Klimowicz, S. and Callot, J.P., 2021. Burial-deformation history of folded rocks unraveled by fracture analysis, stylolite paleopiezometry and vein cement geochemistry: a case study in the Cingoli Anticline (Umbria-Marche, Northern Apennines). Geosciences, 11(3), p.135.
29. Labeur, A., Beaudoin, N.E., Lacombe, O., Gout, C. and Callot, J.P., 2024. Constraining the onset of orogenic contraction in fold-and-thrust belts using sedimentary stylolite populations (Umbria-Marche Apennines, Italy). Journal of Structural Geology, 182, p.105098.
30. Lacombe, O., Beaudoin, N.E., Hoareau, G., Labeur, A., Pecheyran, C. and Callot, J.P., 2021. Dating folding beyond folding, from layer-parallel shortening to fold tightening, using mesostructures: lessons from the Apennines, Pyrenees, and Rocky Mountains. *Solid Earth*, *12*(10), pp.2145-2157.

 doi:10.20944/preprints202506.0230.v1

31. Magni, S., Martín-Martín, J.D., Bons, P.D. and Gomez-Rivas, E., 2025. Stylolites in Carbonate Rocks: Morphological Variability According to the Host Rock Texture. *Minerals*, *15*(2), p.132.
32. Mishra, D.C. and Kumar, S.R., 1998. Characteristics of faults associated with Narmada–Son lineament and rock types in Jabalpur sector. *Current Science*, pp.308-310.
33. Murty, T.V.V.G.R.K. and Mishra, S.K., 1981. The Narmada-Son lineament and the structure of the Narmada rift system. *Journal Geological Society of India*, *22*(3), pp.112-120.
34. Park, W.C. and Schot, E.H., 1968. Stylolites; their nature and origin. *Journal of Sedimentary Research*, *38*(1), pp.175-191.
35. Patro, B.P.K. and Sarma, S.V.S., 2007. Trap thickness and the subtrappean structures related to mode of eruption in the Deccan Plateau of India: results from magnetotellurics. *Earth, planets and space*, *59*, pp.75-81.
36. Railsback, L.B., 1993. Lithologic controls on morphology of pressure-dissolution surfaces (stylolites and dissolution seams) in Paleozoic carbonate rocks from the mideastern United States. *Journal of Sedimentary Research*, *63*(3), pp.513-522.
37. Ravi Shanker 1987. Neotectonic Activity along the Tapti-Satpura Lineament in Central India. Ind. Min, 41 (1): 19-30.
38. Regnet, J.B., David, C., Robion, P. and Menéndez, B., 2019. Microstructures and physical properties in carbonate rocks: A comprehensive review. *Marine and Petroleum Geology*, *103*, pp.366-376.
39. Renard, F., Schmittbuhl, J., Gratier, J.P., Meakin, P. and Merino, E., 2004. Three-dimensional roughness of stylolites in limestones. *Journal of Geophysical Research: Solid Earth*, *109*(B3).
40. Rolland, A., Toussaint, R., Baud, P., Conil, N. and Landrein, P., 2014. Morphological analysis of stylolites for paleostress estimation in limestones. International Journal of Rock Mechanics and Mining Sciences, 67, pp.212-225.
41. Rolland, Y., Perincek, D., Kaymakci, N., Sosson, M., Barrier, E. and Avagyan, A., 2012. Evidence for~ 80–75 Ma subduction jump during Anatolide–Tauride–Armenian block accretion and~ 48 Ma Arabia–Eurasia collision in lesser caucasus–East Anatolia. Journal of Geodynamics, 56, pp.76-85.
42. Ruidas, D.K. and Zijlstra, J.J.P., 2023. The hardgrounds of the Turonian–Coniacian carbonates of the Bagh Group of central India. *Journal of Earth System Science*, *132*(1), p.27.
43. Ruidas, D.K., Paul, S. and Gangopadhyay, T.K., 2018. A reappraisal of stratigraphy of Bagh Group of rocks in Dhar District, Madhya Pradesh with an outline of origin of nodularity of Nodular Limestone Formation. *Journal of the Geological Society of India*, *92*, pp.19-26.
44. Ruidas, D.K., Pomoni-Papaioannou, F.A., Banerjee, S. and Gangopadhyay, T.K., 2020. Petrographical and geochemical constraints on carbonate diagenesis in an epeiric platform deposit: Late Cretaceous Bagh Group in central India. *Carbonates and Evaporites*, *35*, pp.1-21.
45. Rustichelli, A., Tondi, E., Korneva, I., Baud, P., Vinciguerra, S., Agosta, F., Reuschlé, T. and Janiseck, J.M., 2015. Bedding-parallel stylolites in shallow-water limestone successions of the Apulian Carbonate Platform (central-southern Italy). *Italian Journal of Geosciences*, *134*(3), pp.513-534.
46. Schmittbuhl, J., Renard, F., Gratier, J.P. and Toussaint, R., 2004. Roughness of stylolites: implications of 3D high resolution topography measurements. *Physical Review Letters*, *93*(23), p.238501.
47. Self, S., Mittal, T., Dole, G. and Vanderkluysen, L., 2022. Toward understanding Deccan volcanism. *Annual Review of Earth and Planetary Sciences, 50(1),* pp.477-506.
48. Shanker, R., 1991. Thermal and Crustal Structure of" SONATA". A Zone of Mid Continental Rifting in Indian Shield. *Journal Geological Society of India*, *37*(3), pp.211-220.
49. Sridhar, A.R. and Tewari, H.C., 2001. Existence of a sedimentary graben in the western part of Narmada zone: seismic evidence. *Journal of Geodynamics*, *31*(1), pp.19-31.

 doi:10.20944/preprints202506.0230.v1

50. Stockdale, P.B., 1921. *Stylolites: their nature and origin* (Vol. 9). Bloomington, Ind.: sn.
51. Stockdale, P.B., 1943. Stylolites, primary or secondary? *Journal of Sedimentary Research*, *13*(1), pp.3-12.
52. Tewari, H.C., 2001. A tectonic model of the Narmada region. *Current Science*, *80*, pp.873-878.
53. Toussaint, R., Aharonov, E., Koehn, D., Gratier, J.P., Ebner, M., Baud, P., Rolland, A. and Renard, F., 2018. Stylolites: A review. Journal of Structural Geology, 114, pp.163-195.
54. Valdiya, K.S. and Sanwal, J., 2017. Satpura horst and Narmada–Tapi grabens. In Developments in Earth Surface Processes (Vol. 22, pp. 237-247). Elsevier.
55. Whitaker, F.F., Smart, P.L. and Jones, G.D., 2004. Dolomitization: from conceptual to numerical models.
56. Wright, K., Cygan, R.T. and Slater, B., 2001. Structure of the (101 [combining macron] 4) surfaces of calcite, dolomite and magnesite under wet and dry conditions. *Physical Chemistry Chemical Physics*, *3*(5), pp.839-844.
57. Zeboudj, A., Bah, B., Lacombe, O., Beaudoin, N.E., Gout, C., Godeau, N., Girard, J.P. and Deschamps, P., 2023. Depicting past stress history at passive margins: A combination of calcite twinning and stylolite roughness paleopiezometry in supra-salt Sendji deep carbonates, Lower Congo Basin, west Africa. Marine and Petroleum Geology, 152, p.106219.